Inorg. Chem. **2004**, *43*, 116–131

Higher Order Speciation Effects on Plutonium L_3 X-ray Absorption Near Edge Spectra

Steven D. Conradson,*,† Kent D. Abney,‡ Bruce D. Begg,§ Erik D. Brady,|| David L. Clark,⊥ Christophe den Auwer,# Mei Ding,|| Peter K. Dorhout,¶ Francisco J. Espinosa-Faller,¢ Pamela L. Gordon,|| Richard G. Haire,▽ Nancy J. Hess,£ Ryan F. Hess,‡ D. Webster Keogh,⊥ Gerard H. Lander,◇ Anthony J. Lupinetti,‡ Luis A. Morales,‡ Mary P. Neu,|| Phillip D. Palmer,|| Patricia Paviet-Hartmann,|| Sean D. Reilly,|| Wolfgang H. Runde,|| C. Drew Tait,|| D. Kirk Veirs,‡ and Franck Wastin◇

Materials Science and Technology Division, Nuclear Materials Technology Division, Chemistry Division, and Seaborg Institute for Transactinum Studies, Los Alamos National Laboratory, Los Alamos, New Mexico 87545, Australian Nuclear Science and Technology Organisation, Menai, NSW 2234, Australia, CEA Marcoule, 30207 Bagnols sur Ceze Cedex, France, Department of Chemistry, Colorado State University, Fort Collins, Colorado 80523, School of Engineering and Science, Merista University, Centro Marista de Estudios Superiores, Merida, Yucatan, Mexico, Oak Ridge National Laboratory, Oak Ridge, Tennessee 37831, Pacific Northwest National Laboratory, Richland, Washington 99352, and European Commission, Joint Research Centre, Institute for Transuranium Elements, 76125 Karlsruhe, Germany

Received June 10, 2003

Pu L_3 X-ray near edge absorption spectra for Pu(0–VII) are reported for more than 60 chalcogenides, chlorides, hydrates, hydroxides, nitrates, carbonates, oxy-hydroxides, and other compounds both as solids and in solution, and substituted in zirconolite, perovskite, and borosilicate glass. This large database extends the known correlations between the energy and shape of these spectra from the usual association of the XANES with valence and site symmetry to higher order chemical effects. Because of the large number of compounds of these different types, a number of novel and unexpected behaviors are observed, such as effects resulting from the medium and disorder that can be as large as those from valence.

Introduction

When a scanned X-ray comes into resonance with a core electron, an abrupt increase in the absorption occurs, termed the absorption edge. Closer inspection of these edges shows that their features are influenced by the chemical speciation of the absorbing element. X-ray absorption near edge spectroscopy (or structure) (XANES) is analogous to standard UV−vis absorption (and related) spectroscopies in that it follows dipole selection rules. It differs, however, in the 4 orders of magnitude higher energies in the X-ray region and the dominance by continuum instead of bound final states in the case of actinides. Reports assigning most spectral features to transitions with bound final states[1−8] (the $2p_{3/2}$

* To whom correspondence should be addressed at MST-8 MS G755, Los Alamos National Laboratory, Los Alamos, NM 87545. E-mail: conradson@lanl.gov. Phone: (505) 667-9584. Fax: (505) 667-8021.

† Materials Science and Technology Division, Los Alamos National Laboratory.

‡ Nuclear Materials Technology Division, Los Alamos National Laboratory.

§ Australian Nuclear Science and Technology Organization.

|| Chemistry Division, Los Alamos National Laboratory.

⊥ Seaborg Institute for Transactinium Studies, Los Alamos National Laboratory.

CEA Marcoule.

¶ Colorado State University.

¢ Merista University.

▽ Oak Ridge National Laboratory.

£ Pacific Northwest National Laboratory.

◇ Institute for Transuranium Elements.

(1) Bertram, S.; Kaindl, G.; Jove, J.; Pages, M. *Physica B* **1989**, *158*, 508.

(2) Bertram, S.; Kaindl, G.; Jove, J.; Pages, M.; Gal, J. *Phys. Rev. Lett.* **1989**, *63*, 2680.

(3) Heald, S. M.; Tranquada, J. M.; Moodenbaugh, A. R.; Xu, Y. W. *Phys. Rev.* **1988**, *B38*, 761.

(4) Kalkowski, G.; Kaindl, G.; Bertram, S.; Schmiester, G.; Rebizant, J.; Spirlet, J. C.; Vogt, O. *Solid State Commun.* **1987**, *64*, 193.

(5) Kalkowski, G.; Kaindl, G.; Brewer, W. D.; Krone, W. *Phys. Rev.* **1987**, *B35*, 2667.

(6) Petiau, J.; Calas, G.; Petitmaire, D.; Bianconi, A.; Benfatto, M.; Marcelli, A. *Phys. Rev.* **1986**, *B34*, 7350.

(7) Shadle, S. E.; Hedman, B.; Hodgson, K. O.; Solomon, E. I. *J. Am. Chem. Soc.* **1995**, *117*, 2259.

10.1021/ic0346477 CCC: $27.50
Published on Web 12/09/2003

→ 6d for An L_3 edges) are thus frustrated by the 10−15 eV width of the absorption edge relative to the few electronvolts that typically separate the highest energy occupied electronic state and the ionization threshold. An alternative and more accurate model places the ionization threshold near the onset of the absorption jump in the edge region and interprets the main absorption peak as a combination of the atomic-like transition to the continuum, the first extended X-ray absorption fine structure (EXAFS) oscillation, and low energy, undamped multiple scattering (outer well) resonances of the correct symmetry.[9−12] The bound state transitions are therefore confined to the small "pre-edge" features observed for several first row transition metals and other elements.[10,13,14] There are, however, still examples such as Pt L edges where the large peaks at the edge, or white lines, appear to be more successfully described as 2p → 5d transitions and therefore occur below the ionization energy and are affected by HOMO occupancy rather than local geometry.[15,16] Despite the advanced state of spectral calculations and its widespread applicability in many areas, unresolved issues in the interpretation of XANES remain. In addition to the nature of the transition giving the main absorption peak, another of these is chemical transferability, i.e., the extent to and mechanisms by which the chemical speciation may modify the spectra of a given element over its various electronic configurations.

$L_{II,III}$ XANES of Actinides. There is an extensive literature on the application of XANES to actinide chemistry, involving both the utilitarian aspects of determining valence[17−29] and the scientific challenge of interpreting and calculating the spectra.[1,2,4,5,9,28,30−39] The L edges of the lower actinides (Th−Am) exhibit virtually identical correlations between speciation and spectral features for the many accessible valences across the more stable actinides on the left side of their row, and are also useful in addressing actinide environmental chemistry problems via the valence/solubility correlation. Another reason for their widespread application may be that lifetime broadening at their relatively high energies (16−19 keV) renders them relatively featureless and thus easy to interpret, compared to, e.g., first row transition metals. Their principal characteristics are the energies of their features, whether inflection points or peaks, and the behavior of the second shoulder or peak associated with oxo groups when it occurs. Despite, or because of, this paucity of information, the literature cited demonstrates the utility of and interest in these spectra.

Effects of Valence and Charge on Edge Energy. The primary determinant of the absorption edge energy, i.e., the ionization energy and the transition of the core electron to the continuum, is the charge on the central atom. It is, however, essential to distinguish the actual charge from the valence, since it will be modified by the extent of electron transfer from the ligands. In the case of actinides that display valences ≥(V) in equilibrium with H_2O, the monotonic increase in edge energy with valence displays a discontinuity on going from An(IV) to An(V). This is coupled with the formation of the trans dioxo moiety in the higher valence.[1,2,31,40] The multiply bound O atoms at very short An−O distances donate sufficient electron density back to the An atom so that the edge energy is typically about 1 eV lower in the (V) than in the (IV) state, prior to resuming its upward trend from (V) to (VI).

Spectral Intensities and the Ionization Energy. Although there is still some controversy over the position of the ionization threshold with respect to the absorption edge and the origin of the edge features, it is generally accepted that for many elements, and certainly for actinides, the ionization energy is near the bottom of the edge.[9,10] The edge features therefore belong to the extended X-ray absorption fine

(8) Rothe, J.; Denecke, M. A.; Neck, V.; Muller, R.; Kim, J. I. *Inorg. Chem.* **2002**, *41*, 249.
(9) Ankudinov, A. L.; Conradson, S. D.; de Leon, J. M.; Rehr, J. J. *Phys. Rev.* **1998**, *B57*, 7518.
(10) Ankudinov, A. L.; Ravel, B.; Rehr, J. J.; Conradson, S. D. *Phys. Rev.* **1998**, *B58*, 7565.
(11) Rehr, J. J.; Ankudinov, A. L. *J. Electron Spectrosc. Relat. Phenom.* **2001**, *114*, 1115.
(12) Rehr, J. J.; Ankudinov, A. L. *J. Synchrotron Radiat.* **2001**, *8*, 61.
(13) Shadle, S. E.; Hedman, B.; Hodgson, K. O.; Solomon, E. I. *Inorg. Chem.* **1994**, *33*, 4235.
(14) Qian, Q.; Tyson, T. A.; Kao, C. C.; Croft, M.; Cheong, S. W.; Greenblatt, M. *Phys. Rev.* **2000**, *B62*, 13472.
(15) Ankudinov, A. L.; Rehr, J. J.; Low, J. J.; Bare, S. R. *Top. Catal.* **2002**, *18*, 3.
(16) Horsley, J. A. *J. Chem. Phys.* **1982**, *76*, 1451.
(17) Bolvin, H.; Wahlgren, U.; Moll, H.; Reich, T.; Geipel, G.; Fanghanel, T.; Grenthe, I. *J. Phys. Chem. A* **2001**, *105*, 11441.
(18) Bonhoure, I.; den Auwer, C.; Moulin, C. C. D.; Moisy, P.; Berthet, J. C.; Madic, C. *Can. J. Chem.* **2000**, *78*, 1305.
(19) Clark, D. L.; Conradson, S. D.; Ekberg, S. A.; Hess, N. J.; Janecky, D. R.; Neu, M. P.; Palmer, P. D.; Tait, C. D. *New J. Chem.* **1996**, *20*, 211.
(20) Duff, M. C.; Hunter, D. B.; Triay, I. R.; Bertsch, P. M.; Reed, D. T.; Sutton, S. R.; Shea-McCarthy, G.; Kitten, J.; Eng, P.; Chipera, S. J.; Vaniman, D. T. *Environ. Sci. Technol.* **1999**, *33*, 2163.
(21) Hess, N. J.; Weber, W. J.; Conradson, S. D. *J. Alloys Compd.* **1998**, *271*, 240.
(22) Jollivet, P.; den Auwer, C.; Simoni, E. *J. Nucl. Mater.* **2002**, *301*, 142.
(23) Morris, D. E.; Allen, P. G.; Berg, J. M.; Chisholm-Brause, C. J.; Conradson, S. D.; Donohoe, R. J.; Hess, N. J.; Musgrave, J. A.; Tait, C. D. *Environ. Sci. Technol.* **1996**, *30*, 2322.
(24) Moyes, L. N.; Jones, M. J.; Reed, W. A.; Livens, F. R.; Charnock, J. M.; Mosselmans, J. F. W.; Hennig, C.; Vaughan, D. J.; Pattrick, R. A. D. *Environ. Sci. Technol.* **2002**, *36*, 179.
(25) Nitsche, H. *J. Alloys Compd.* **1995**, *223*, 274.
(26) Panak, P. J.; Booth, C. H.; Caulder, D. L.; Bucher, J. J.; Shuh, D. K.; Nitsche, H. *Radiochim. Acta* **2002**, *90*, 315.
(27) Silva, R. J.; Nitsche, H. *Radiochim. Acta* **1995**, *70*, 377.
(28) Williams, C. W.; Blaudeau, J. P.; Sullivan, J. C.; Antonio, M. R.; Bursten, B.; Soderholm, L. *J. Am. Chem. Soc.* **2001**, *123*, 4346.
(29) Reich, T.; Bernhard, G.; Geipel, G.; Funke, H.; Hennig, C.; Roseberg, A.; Matz, W.; Schell, N.; Nitsche, H. *Radiochim. Acta* **2000**, *88*, 633.
(30) Allen, P. G.; Veirs, D. K.; Conradson, S. D.; Smith, C. A.; Marsh, S. F. *Inorg. Chem.* **1996**, *35*, 2841.
(31) Conradson, S. D.; Al Mahamid, I.; Clark, D. L.; Hess, N. J.; Hudson, E. A.; Neu, M. P.; Palmer, P. D.; Runde, W. H.; Tait, C. D. *Polyhedron* **1998**, *17*, 599.
(32) den Auwer, C.; Madic, C.; Berthet, J. C.; Ephritikhine, M.; Rehr, J. J.; Guillaumont, R. *Radiochim. Acta* **1997**, *76*, 211.
(33) den Auwer, C.; Simoni, E.; Conradson, S. D.; de Leon, J. M.; Moisy, P.; Beres, A. *C. R. Acad. Sci., Ser. IIc: Chim.* **2000**, *3*, 327.
(34) Hudson, E. A.; Allen, P. G.; Terminello, L. J.; Denecke, M. A.; Reich, T. *Phys. Rev.* **1996**, *B54*, 156.
(35) Hudson, E. A.; Rehr, J. J.; Bucher, J. J. *Phys. Rev.* **1995**, *B52*, 13815.
(36) Lissner, F.; Kramer, K.; Schleid, T.; Meyer, G.; Hu, Z. W.; Kaindl, G. *Z. Anorg. Allg. Chem.* **1994**, *620*, 444.
(37) van den Berghe, S.; Verwerft, M.; Laval, J. P.; Gaudreau, B.; Allen, P. G.; van Wyngarden, A. *J. Solid State Chem.* **2002**, *166*, 320.
(38) Yang, C. Y.; Johnson, K. H.; Horsley, J. A. *J. Chem. Phys.* **1978**, *68*, 1001.
(39) Allen, P. G.; Bucher, J. J.; Shuh, D. K.; Edelstein, N. M.; Reich, T. *Inorg. Chem.* **1997**, *36*, 4676.
(40) Antonio, M. R.; Soderholm, L.; Williams, C. W.; Blaudeau, J. P.; Bursten, B. E. *Radiochim. Acta* **2001**, *89*, 17.

structure (EXAFS) region and will be determined by the local structure around the central atom that defines the photoelectron scattering paths and not by, in the case of An $L_{II,III}$ XANES, the 6d occupancy. In this scheme, the principal absorption peak in the An $L_{II,III}$ XANES is the first EXAFS oscillation superimposed on the atomic absorption that rises in coincidence. Larger numbers of nearest neighbor atoms and shorter distances may therefore increase the peak amplitude because of the *N* (number of neighbor atoms in a shell) and inverse r^2 (r = absorber scatterer distance) factors. Longer An−nearest neighbor distances that increase the frequency of this most important EXAFS wave might therefore shift the absorption edge (but not necessarily the ionization energy) to lower energy. If the local environment contains more than one nearest neighbor shell, then the effects on the XANES will also be complicated, since the *N* and *r* dependence of the EXAFS for these shells will influence the XANES. Two of the most distinctive features of An $L_{II,III}$ XANES are therefore the decrease in the height of the main peak and the appearance of the shoulder on its high energy side that occur in the spectra of An($\geq$ 5) bis-oxo complexes and reflect the two different An−O distances.[9,34,35] The relative prominence of this shoulder continues to increase in tetra-oxo complexes, but also in actinate compounds of which at least some exhibit only a single An−O nearest neighbor distance where two mechanisms have been proposed to account for this characteristic.[41,42]

Spectral Intensities and Local Geometry. Implicit in this interpretation, however, are also the "outer well" states. These are discrete states of the low kinetic energy, quasibound photoelectron within the potential well of the nearest neighbor atoms and are thus equivalent to multiple scattering resonances in the EXAFS formalism. In common with final states localized on the absorber, these transitions will be highly sensitive to the initial and final state symmetries, with the latter defined by the coordination geometry. It is also perhaps worth speculating whether these states could overlap with occupied ones of the neighbors. If so, then this would provide a mechanism for reducing the transition cross section, and corresponding spectral amplitude, that is identical to the description involving electron donation from the ligand to the absorber highest occupied state. This correlation between spectral amplitude and the occupancy of high lying states is one of the more appealing features of the assignment of the XANES peak to the bound state. Direct donation into the quasibound state would be more consistent with the location of the ionization energy near the base of the edge and assignment of the peak to transitions to unbound final states of d symmetry.

Although these factors are understood qualitatively, little work, which if most rigorous would include comparisons of photoemission and XANES data, has been done to quantify the effects of different types of ligands and bonding. Many of the research groups active in this field have reported on experimental and theoretical aspects for either a single class of compounds or a limited number of spectra across more than one class. What is lacking, however, is a concerted attempt to explore the boundaries or envelope of the XANES by exploiting the wide range of compounds and valences and the conditions over which they exist. It is therefore of interest to examine changes in the XANES as the ligands are varied, especially with respect to changes associated directly with the valence. We report herein such an examination for the Pu L_3 edge for Pu(0−VII), including chalcogenides and other low valence solids, aquo, hydroxo, nitrato, and carbonato complexes in acidic and basic media, aquochloride complexes in acid, and oxo, hydroxo, and aquo solids related to the cubic PuO_2. Spectra from more compounds than the 50+ listed were obtained. Results from these were not reported if they simply duplicated those from a class that was already well represented. Although it would be possible to calculate many of these spectra for comparison with experiment, it is outside the scope of this paper to attempt to understand the origins of the observed effects outside of a few purely empirical structure/spectrum relationships.

Materials and Methods

PuS, PuSe, PuTe, and PuN were prepared and characterized by standard methods.[43−45]

PuB_4 was prepared analogously to the uranium compound.[46] The Pu compound used was not stoichiometric but a mixture of the tetra- and diborides.

PuS_2, Pu_2S_3, $PuSe_2$, and Pu_2Se_3 were synthesized by loading stoichiometric amounts of plutonium metal and elemental chalcogen in a fused silica ampule sealed under vacuum. The ampules were then heated to 500 °C over 16 h and held there for 48 h. In all cases, the plutonium chalcogenide products had a dull black appearance and were polycrystalline.[44,47,48]

Highly ordered PuO_2 was formed during the attempted measurement of KPu_2Se_6, prepared from a mixture of 0.0480 g (0.20 mmol) of Pu, 0.0320 g (0.41 mmol) of Se, and 0.3160 g (0.80 mmol) of K_2Se_4. The mixture was loaded into a fused silica ampule and sealed under vacuum. The ampule was then heated to 500 °C over 16 h and held there for 200 h. The ampule was cooled to ambient temperature at a rate of 3 °C per hour. Excess flux was removed by washing with DMF.[47] Black rectangular blocks with a metallic luster were then isolated by handpicking and used for XAFS analysis by grinding with a mortar and pestle with BN in air prior to loading into the sealed holder. Having followed this procedure, the XAFS spectrum was not that of the target selenide but rather the most highly ordered PuO_2 ever observed. The Se XAFS also did not show neighboring Pu. Repeating this entire sequence gave identical results. We believe that under these conditions the Pu reacts with O from the silica and similar sources so that, in the

(41) Van den Berghe, S.; Verwerft, M.; Laval, J. P.; Gaudreau, B.; Allen, P. G.; Van Wyngarden, A. *J. Solid State Chem.* **2002**, *166*, 320.
(42) de Leon, J. M.; Conradson, S. D.; Clark, D. L.; den Auwer, C.; Hess, N. J. *Inorg. Chem.*, submitted.
(43) Gouder, T.; Wastin, F.; Rebizant, J.; Havela, L. *Phys. Rev. Lett.* **2000**, *84*, 3378.
(44) Katz, J. J.; Seaborg, G. T.; Morss, L. R. *The Chemistry of the Actinide Elements*; Chapman and Hall: New York, 1986; Vol. 1.
(45) Wachter, P.; Marabelli, F.; Bucher, B. *Phys. Rev.* **1991**, *B43*, 11136.
(46) Lupinetti, A. J.; Fife, J. L.; Garcia, E.; Dorhout, P. K.; Abney, K. D. *Inorg. Chem.* **2002**, *41*, 2316.
(47) Hess, R. F. Thesis, Investigation Into the Fundamental Solid-State Chemistry of the Actinide Elements: Synthesis and Characterization of Actinide Chalcogenide Compounds, Colorado State University, 2001.
(48) Marcon, J. P.; Pascard, R. *J. Inorg. Nucl. Chem.* **1966**, *28*, 2551.

absence of any exposure to H_2O and with the long reaction time, the highly ordered PuO_2 product results.

The aquo complexes in 1 M $HClO_4$ have been reported previously.[31] These spectra were reanalyzed using improved calibration and normalization methods for this report.

Pu(IV) chloride complexes were prepared as follows. Pu(IV) in acidic solution was purified to remove Am and other metal ions using an anion-exchange resin (Lewatite MP-500) that binds Pu(IV) as $Pu(Cl)_6^{2-}$. The Pu(IV) was eluted with 1.0 M HCl. The stock solutions were assayed using UV−vis−near-IR spectroscopy to verify the oxidation state purity and solution concentration. The Pu(IV) oxidation state was confirmed and plutonium content assayed by using a characteristic absorbance band at 470 nm (ϵ = 58 M^{-1} cm^{-1}). Aliquots of this stock solution were diluted into solutions of varying HCl, NaCl, and $NaClO_4$ concentrations to yield a range of Pu(IV) chloro complexes in constant ionic strength solution.

Crystalline $(Et_4N)_2PuCl_6$ was prepared from the Pu(IV) stock solution described above. An aliquot of Pu(IV)−1.0 M HCl stock solution was added to an ethanol solution containing 2 equiv of tetraethylammonium chloride. The solvent was evaporated slowly to yield single crystals for X-ray diffraction analysis. Approximately 2 mg of the crystals was ground and combined with BN for XAFS analysis.

Pu(VI) chloride complexes in acidic solution were prepared as described.[49]

Pu(IV) nitrato complexes in HNO_3 solution were prepared as described.[50]

Pu(IV, V, and VI) carbonato complexes and crystals were prepared as described.[51,52]

Pu hydroxide complexes were prepared as described.[53,54]

Colloidal Pu(IV) oxo-hydroxides were prepared by variations on the reported method.[55−57] Nitrate-based colloidal Pu(IV) hydroxide ("nitrate colloid") was prepared as follows. A Pu(IV) stock solution was prepared by dissolving Pu metal in 4 M $HClO_4$ and assayed for Pu(IV) using optical absorbance spectroscopy. A 0.52 mL aliquot of the resulting 0.76 M Pu stock solution was added to 3.0 mL of 4.0 M HNO_3. The pH of the resultant solution was raised to 6 using concentrated NH_4OH and then to 9.15 using 25% NH_4-OH to yield a finely divided, emerald green precipitate. The solid was washed with distilled, deionized water six times and peptized in 0.08 M HNO_3. After heating at 82 °C for 8 h and adding 0.5 mL of 8 M HNO_3, approximately 75% of the material was suspended in solution as determined using previously determined extinction coefficients for colloidal Pu(IV) hydroxide formed under similar conditions. The final solution pH was 1.7. The suspension was centrifuged at 7000 rpm for 10 min; an aliquot from the top of the solution column was sampled for XAFS measurements, which were performed at ambient temperature. Light scattering and field flow fractionation showed a broad, 20−200 Å range of particle sizes. Electron microscopy shows polymer-like, amorphous morphology. X-ray and electron diffraction give the *Fm*3*m* pattern of PuO_2, but with very broad peaks indicative of small crystallite sizes. Such crystallites in suspension can aggregate into micron-scale particles.

Nitrate-based colloidal Pu(IV) hydroxide in saturated NaCl ("nitrate + NaCl") was prepared as described above with the addition of NaCl to the HNO_3 solution. For this sample, 0.050 mL of the 0.76 M Pu, 4 M $HClO_4$ stock solution was added to 3.0 mL of 4.0 M HNO_3, saturated NaCl solution. The final solution pH was 1.9. XAFS measurements on this sample were also made on the suspension at ambient temperature. Nitrate-based colloidal Pu(IV) hydroxide in citrate ("nitrate + citrate") was made analogously.

Aged colloids were prepared by precipitating a Pu(IV) nitrate solution (~1 M HNO_3) with an excess of strong base, and the resulting precipitate washed repeatedly (6−10×) with triple distilled water. The precipitate was then peptized in dilute HNO_3 with a NO_3^-/Pu ratio of ~0.8. It was maintained in suspension for five years, after which it was slowly dried to a solid by evaporation at room temperature. Electron microscopy showed particle sizes of 15−20 Å. The NO_3^-/Pu ratio was 0.8. This sample was resuspended in H_2O for the XAFS measurements at ambient temperature.

A second sample prepared by the same procedure was hydrothermally treated at 240 °C to increase the crystallite size and reduce the NO_3^-/Pu ratio to ~0.08. It was also maintained in suspension for several years and then dried. The particle size of this material was 75−80 Å, and it did not originally display secondary aggregation. The NO_3^-/Pu ratio was 0.1. This material was resuspended by heating at 80 °C for 2 h, followed by sonication for 2 h. This treatment only put about half the sample back into suspension. The XAFS sample ("aged hydrothermal") was taken from the supernate, which was redried, loaded as the solid, and measured at 80 K.

Colloidal Pu(IV) oxy-hydroxides were also prepared by heterogeneous reduction in brine ("reduced (VI)" samples). A 1 mL portion of 0.01 M Pu(VI) hydrochloride solution with pH ~ 2 was added to a 15 mL glass vial charged with 3.6 mL of 5 M NaCl and 0.4 mL of 0.01 M NaOH (in the case of ERDA, the glass vial was charged with 2 mL of ERDA, 1 mL of 0.1 M HCl, and 1 mL of 0.01 N NaOH) and mixed well. For samples prepared with NaOCl, 1 mL of 0.01 mL Pu(VI) hydrochloride solution with pH ~ 2 was added into a 15 mL glass vial charged with 3 mL of 5 M NaCl and 1 mL of 0.005 M NaOCl (in the case of ERDA, the glass vial was charged with 2 mL of ERDA, 1 mL of 0.1 M HCl, and 1 mL of 0.005 M NaOCl) and mixed well. Either 0.5 g Fe or Al powder (both <10 μm) was subsequently added to the solution. The solution and Fe/Al powder were contacted by shaking for 30 days. After 30 days, the mixture was transferred to centrifuge tubes and spun down. The supernatant was pipetted into a clean tube and capped. The residue was then transferred into a sample holder for XAFS experiments. ERDA is a synthetic brine intended to duplicate conditions at the Waste Isolation Pilot Plant Site and contains 248.6

(49) Runde, W. H.; Neu, M. P.; Conradson, S. D.; Clark, D. L.; Palmer, P. D.; Reilly, S. D.; Tait, C. D. *Spectroscopic Investigation of Actinide Speciation in Concentrated Chloride Solution*; Materials Research Society Symposium Proceedings Scientific Basis for Waste Management XX; Materials Research Society: Warrendale, PA, 1996.
(50) Veirs, D. K.; Smith, C. A.; Berg, J. M.; Zwick, B. D.; Marsh, S. F.; Allen, P. G.; Conradson, S. D. *J. Alloys Compd.* **1994**, *213*, 328.
(51) Clark, D. L.; Conradson, S. D.; Keogh, D. W.; Neu, M. P.; Palmer, P. D.; Runde, W. H.; Scott, B. L.; Tait, C. D. *X-ray Absorption and Diffraction Studies of Monomeric Actinide Tetra-, Penta-, and Hexa-Valent Carbonato Complexes*; NEA Proceedings of the Workshop on Speciation, Techniques, and Facilities for Radioactive Materials at Synchrotron Light Sources; Grenoble, France, 1998.
(52) Clark, D. L.; Conradson, S. D.; Keogh, D. W.; Palmer, P. D.; Scott, B. L.; Tait, C. D. *Inorg. Chem.* **1998**, *37*, 2893.
(53) Brady, E. D.; Clark, D. L.; Conradson, S. D.; Dewey, H. J.; Donohoe, R. J.; Gordon, P. L.; Konze, W. V.; Keogh, D. W.; Palmer, P. D.; Tait, C. D. *Inorg. Chem.*, in preparation.
(54) Peretrukhin, V. F.; Shilov, V. P.; Pikaev, A. K. *Alkaline Chemistry of Transuranium Elements and the Treatment of Alkaline Radioactive Wastes*; WHC-EP-0817; Westinghouse Hanford Company: Richland, VA, May 1995.
(55) Bell, J. T.; Coleman, C. F.; Costanzo, D. A.; Biggers, R. E. *J. Inorg. Nucl. Chem.* **1973**, *35*, 629.
(56) Lloyd, M. H.; Haire, R. G. *Radiochim. Acta* **1978**, *25*, 139.
(57) Hobart, D. E.; Morris, D. E.; Palmer, P. D.; Newton, T. W. *Proceedings of The Topical Meeting on Nuclear Waste Isolation in the Unsaturated Zone: FOCUS'89*; Los Alamos National Laboratory Report LA-UR-89-2541; Las Vegas, Nevada, 1989.

g of NaCl, 22.52 g of Na_2SO_4, 5.70 g of $Na_2B_4O_7 \cdot 10\ H_2O$, 1.074 g of NaBr, 6.869 g of KCl, 3.667 g of $MgCl_2 \cdot 6H_2O$, and 1.672 g of $CaCl_2 \cdot 2H_2O$ per liter of solution.

PuO_{2+x} type compounds were prepared by oxidation of PuO_2 or Pu metal with H_2O at elevated temperature as follows. The PuO_2 starting material (high fired a) was synthesized by the oxidation of doubly refined α plutonium metal. The typical metallic impurities are on the order of 400 ppm. The oxide was fired in air at 1000 °C. The lattice constant was consistent with $PuO_{1.97}$. $PuO_{2.17}$, $PuO_{2.21}$, and $PuO_{2.26}$ were prepared by the reaction of PuO_2 high fired (a) with H_2O vapor at 300 °C. The calculated values of $x = 0.17$, $x = 0.21$, and $x = 0.26$ were based on the pressure of H_2 generated during the reaction and assuming that the starting material had $x = 0$. The lattice constants were 5.4022 Å for $x = 0.17$ and 5.4038 Å for $x = 0.26$, corroborating this analysis. High fired PuO_2 was prepared and reacted with H_2O vapor under ambient conditions as follows. Low fired PuO_2 was synthesized by firing Pu metal in air at 800 °C; high fired (b) was prepared by firing Pu metal in air at 1000 °C. High fired (b) was subsequently equilibrated at ambient temperature for two weeks above 28, 51, and 65 wt % H_2SO_4 solutions, which gave 15%, 37%, and 80% relative humidity (rh; referred to as 15rh, 37rh, and 80rh), prior to being loaded in the XAFS sample holders.

$Nd_{0.5}Pu(III)_{0.5}PO_4$, $Ca_{0.8}Pu(III)_{0.2}HfTi_{1.8}Al_{0.2}O_7$, $Ca_{0.8}Pu(IV)_{0.2}HfTi_{1.8}Al_{0.2}O_7$, $Ca_{0.9}Pu(III)_{0.1}Ti_{0.8}Al_{0.2}O_3$, and $Ca_{0.9}Pu(IV)_{0.1}Ti_{0.8}Al_{0.2}O_3$ were prepared as described.[58,59]

Pu in borosilicate glass was prepared as described.[21]

All XAFS measurements were performed at the Stanford Synchrotron Radiation Laboratory, under dedicated operating conditions (3.0 GeV, 50−100 mA), on end stations 4-2 and 11-2. Solid samples were usually held at 80 K; solutions and suspensions were run at ambient temperature. Differences in Debye−Waller factors are expected to have only minor effects on the XANES. Si [220] crystals were used to monochromate the beam. Harmonics were usually eliminated with a flat, Pt-coated mirror with a cutoff energy of 20−25 keV. When no mirror was available, the second crystal of the monochromator was detuned to give 50% of the maximum intensity in the ion chambers that were filled with N_2. The premonochromator vertical slits were set at 0.5−1.0 mm, which is sufficient for the 1 part in 10^4 resolution (2 eV) resolution attainable by the beam line. Since this is much less than the core-hole width, the reported widths of the spectral features can be assumed to be intrinsic and not instrument limited. Data were taken in both transmission and fluorescence modes. Fluorescence was measured with a multielement Ge detector, using analogue or digital amplifiers. For fluorescence data, a dead time type of correction was made to adjust the absorption peak height to match that of the transmission data when applicable. This corrects for self-absorption as well as dead time. Otherwise, dead times of 1−2 μs were used. Spectral features were somewhat broader when measured by fluorescence, which decreased the absorption edge energy by 0−0.3 eV. In most cases, a Zr foil was measured with a third ion chamber coincident with the Pu scan by extending the edge region below the Zr edge. Otherwise, the Zr foil was measured by a separate scan taken just before the Pu scan. The first inflection point of the Zr foil was defined as 17999.35 eV. After the absorbance was calculated, it was normalized by offsetting it so that the value of a second-order polynomial fit through the pre-edge was zero and scaling it so that the value of a third-order polynomial fit through the region above the edge was unity at 18075 eV. The reported peak energies are the zeroes of the first derivative; the edge energies are the inflection points of the absorption edges. Although curve-fitting the XANES to Gaussians (representing individual transitions) plus an arctangent (representing the continuum transition) has often been used as a method for analyzing XANES,[5,31] it is not used here. A more thorough examination of this procedure shows that the location of the arctangent function and therefore the reported ionization energy is actually very sensitive to the range of data used in the fit and therefore reflects aspects of the fitting procedure and not the actual energy of the continuum. This in turn affects the amplitudes and widths of the Gaussians. Since the curve-fitting results are highly dependent on the procedure, poor representations of the physical processes determining the spectrum curve-fitting were avoided in favor of the more straightforward (but less informative) peak and inflection point energies. In addition, since recent theoretical advances point to location of the ionization threshold on the absorption edge and do not assign the absorption peak to a bound (6d) final state, characterizing the peak with a Gaussian is also unphysical.[9,10] Differentiation was performed numerically. For each discrete point, three points on each side (for a total of seven) were fit to a second order polynomial. The value of the derivative at that point was then calculated as two times the quadratic coefficient times the energy plus the linear coefficient. The second derivative was subsequently calculated in this way from the first. The interval between points during the scans was typically 0.8 eV. Since core-hole lifetime broadening for these spectra is of the order of 6 eV, this sampling interval is more than sufficient to ensure intrinsic rather than instrument-limited resolution for these spectra. There have been questions at times as to how the results can be reported to 0.1 eV when the interval between data points is typically 0.8 eV. What is omitted in this simplistic view is that the ability to interpolate the data to determine peak and inflection point energies depends on the sampling interval along the ordinate as well as the abscissa. The relatively coarse separation in energy is balanced by the fine separation in the absorbance signal, which was usually of the order of 500000 counts over the edge in fluorescence (the sum from multiple detectors) or 200000 counts in absorbance. This permits the true shape of the edge to be determined with great precision so that the energies of the features can subsequently be interpolated from the fits of the polynomials to sets of points to much less than the difference in energy between the points. The precision is then derived from the accuracy of the energy determination and the error in the monochromator position and not the energy interval. From our experience with duplicate samples, many of which are included here, the accuracies of the tabulated energies are 0.2−0.5 eV or better, with higher errors occurring in comparing spectra collected in different runs and lower errors for spectra measured during the same run. That is, there can be problems with poorly understood, systematic experimental errors that can affect these results. We note, however, that no conclusions described in this report are based on single results and that all of the trends identified and discussed are strictly monotonic. The credibility of the reported results is therefore greatly enhanced by the use of multiple, independent samples and spectra for each class of compounds.

Results

Because of lifetime broadening and the energy of the ionization threshold relative to the edge jump, Pu L_3 XANES do not show the wealth of features that appear in their M edges or in, e.g., first row transition metal K edges. As a

(58) Begg, B. D.; Vance, E. R.; Conradson, S. D. *J. Alloys Compd.* **1998**, *271−273*, 221.
(59) Begg, B. D.; Vance, E. R.; Day, R. A.; Hambley, M.; Conradson, S. D. *Plutonium and Neptunium Incorporation in Zirconolite*; Scientific Basis for Nuclear Waste Management XX; Pittsburgh, PA, 1997.

result, these Pu spectra tend to be similar in appearance, exhibiting a broad, smooth rise to the single absorption peak followed by a relatively smooth drop (that may show some unresolved features) into the local minimum of the first distinct EXAFS oscillation. The one prominent feature they sometimes display is an unresolved shoulder on the high energy side of the main peak in the spectra of oxo complexes. The principle characteristics reported are therefore the amplitude of the peak, which is the main or primary peak since there is only one, its energy, and the energy of the inflection point of the edge jump that may also be called the edge or absorption edge energy. The reason for not using curve-fits of the XANES to determine peak widths has been described. In addition, shifts in the edge energy are often not accompanied by concomitant changes in the peak energy and the absorbance as it descends from the peak, indicating that such changes may not be simple peak broadening but more complicated, asymmetric modifications to its shape. Nevertheless, the difference between the peak and edge energies may be used as a metric of the width of the main peak.

Aquo Complexes in Noncoordinating Acidic Media. This set of spectra constitutes a baseline for comparison with other compounds. Pu(III,IV), and (VI) were solubilized in aqueous solution by 1 M $HClO_4$. Pu(V) was at pH = 7 with 1 M $NaClO_4$. The (III) and (IV) complexes (**A**) are spherical, with 8−10 aquo ligands. The Pu(V), (VI), and (VII) complexes (**B**) have trans oxo groups with very short bond lengths and equatorial ligands at much longer distances in the plane normal to the oxo axis (Table 1). Since ClO_4^- is noncoordinating, the ligands are expected to be (neutral) H_2O molecules. The effects described in the Introduction are easily observed in the XANES of this aquo complex series, which have been reanalyzed for presentation here with the addition of the Pu(VII) hydroxide complex (Figure 1). In common with the L_3 edge of other actinides, the absorption edge shifts to higher energy with increasing valence, except between Pu(IV) and (V). The peak height is higher for complexes with larger numbers of near neighbors at a single distance, and the two distances in the Pu(V, VI, VII) oxo complexes decrease the peak height and result in a shoulder on the high energy side of the main peak. On closer inspection, the energy shifts with increasing valence, beginning with Pu(0)−(III) are 3.0 eV, 3.2 eV for Pu(III)−(IV), −0.9 eV for Pu(IV)−(V), 2.6 eV for Pu(V)−(VI), and 0.5 eV for Pu(VI)−(VII). In this sequence, the small difference between Pu(VI) and (VII) is indicative of more than just increased electron transfer with higher valence; the Pu(VI)−(VII) shift is modified by the presence of the hydroxide ligands in the (VII) complex. The (VI) hydroxide complex edge (vide infra) is 1.0 eV lower than that of the aquo complex, and the Pu(VI)−(VII) hydroxide edge shift is therefore 1.5 eV. The anomaly is the 1.0 eV/e shift between Pu(0) and (III) (which may actually be even smaller because self-absorbance in the metal spectrum reduces the peak height disproportionately and shifts the inflection point but not the peak to higher energies). This is comparable to the Pu(VI) and (VII) states where the high formal charge of the Pu is adept at pulling

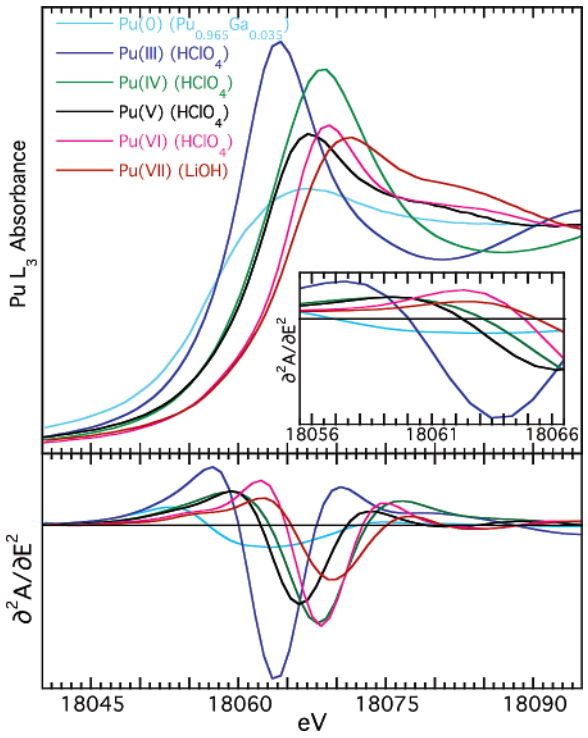

Figure 1. XANES (normalized absorbance, top; second derivative, bottom; expanded zeros of second derivative, inset) of Pu aquo complexes, δ PuGa, and Pu(VII) hydroxide. The second derivative zeros correspond to the inflection points of the absorption edge and are used as the edge energy. The peak amplitude of the PuGa alloy is suppressed by self-absorbance of this opaque sample.

electrons away from the O ligands. The peak energy of the metal is also quite high, because of its width, despite the long Pu−Pu distance and short period of the EXAFS wave from the first shell. It is actually higher than that for the Pu(III) complex, which is, however, lower relative to the peak of the (IV) complex than the inflection points of the edges.

Low Valence Chalcogenides, Halides, and Boride. These compounds are all formally Pu(II), (III), and (IV), but with relatively soft and/or distant ligands and extended structures that promote semiconducting and even metallic behavior. The

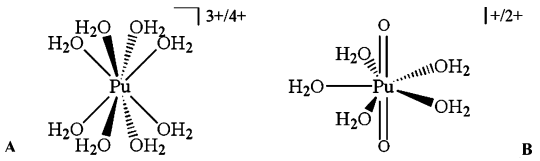

di- and tetravalent chalcogenides are cubic, and even the tetraboride with its layered structure still has the Pu in a high symmetry site. Although the boride is actually a mixture of the tetra- and diborides, the Pu in both is likely to have similar (low) valence and speciation in both compounds. It is therefore included because it is useful to demonstrate that it behaves more like the nitride and chloride than the semiconducting/metallic materials. In most cases the EXAFS only finds a single primary shell of nearest neighbor atoms in agreement with crystallography; the second distances reported in the table refer to shells with relatively small numbers of atoms that would be lattice distortions and not

Table 1. XANES Parameters and Nearest Neighbor Distances[a]

sample	edge energy	ΔeV PuO_2 edge	peak energy	normalized peak height	nearest neighbor Pu−X distances (Å)
		Metallic			
(0) δ $Pu_{0.965}Ga_{0.035}$	18057.0	−5.3	18067.3	na	
		Aquo Complexes ($HClO_4$)			
(III) 1 M $HClO_4$	18060.0	−2.3	18064.3	1.85	2.48
(IV) 1 M $HClO_4$	18063.2	0.9	18068.7	1.72	2.39
(V) $HClO_4$ pH 5.5	18062.3	0.0	18067.6	1.43	1.81, 2.47
(VI) 1 M $HClO_4$	18064.9	2.6	18069.5	1.47	1.75, 2.41
		Chalcogenides/Halides			
(III) 1 M $HClO_4$	18060.0	−2.3	18064.3	1.85	2.48
PuS	18057.2	−5.1	18064.4	1.29	2.78
PuSe	18057.4	−4.9	18064.0	1.31	2.87, 3.25
PuTe	18057.3	−5.1	18065.2	1.30	3.10, 3.44
Pu_2S_3	18057.8	−4.5	18064.1	1.30	2.86
Pu_2Se_3	18058.2	−4.1	18064.0	1.37	3.00
PuN	18059.1	−3.2	18067.2	1.30	(1.91), 2.49
PuB_4	18058.8	−3.5	18065.9	1.32	2.63, 2.97
$PuCl_3$	18059.2	−3.1	18064.7	1.43	2.58, 2.77
PuS_2	18058.0	−4.3	18064.0	1.34	2.81
$PuTe_2$	18058.1	−4.2	18064.0	1.32	2.94, 3.06
$(Et_4N)_2PuCl_6$	18061.4	−0.9	18068.1	1.52	2.60
		Aquo-Chloro Complexes			
(IV) 1 M $HClO_4$	18063.2	0.9	18068.7	1.72	2.39
Pu(IV), 3.5 M HCl, 0.3 Cl^-	18063.7	1.4	18068.6	1.83	2.39, 2.63
Pu(IV), 1.4 M HCl, 0.9 Cl^-	18062.8	0.5	18068.2	1.83	2.39, 2.63
Pu(IV), 7.6 M HCl, 2.9 Cl^-	18062.3	0	18067.7	1.69	2.40, 2.63
Pu(IV), 10.8 M HCl, 5.5 Cl^-	18061.7	−0.6	18068.0	1.58	2.39, 2.61
$(Et_4N)_2PuCl_6$	18061.4	−0.9	18068.1	1.52	2.60
(VI) 1 M $HClO_4$, 4.5 H_2O	18064.9	2.6	18069.5	1.47	1.75, 2.41
Pu(VI), 1 M $HClO_4$ + 1 M NaCl, 3.8 H_2O	18064.9	2.6	18069.6	1.47	1.74, 2.42
Pu(VI), 1 M $HClO_4$ + 4M NaCl, 2.7 H_2O, 1.3 Cl^-	18064.5	2.2	18069.3	1.46	1.75, 2.43, 2.75
Pu(VI), 1 M HCl + 15 M LiCl, 2.6 H_2O, 2.4 Cl^-	18064.1	1.8	18069.5	1.35	1.75, 2.49, 2.70
		(IV) Aquo-nitrato Complexes			
(IV), 1 M $HClO_4$	18063.2	0.9	18068.7	1.72	2.39
Pu(IV), $(NO_3)_2^{2+}$, 3 M HNO_3	18065.4	3.1	18070.1	1.88	2.42
Pu(IV), $(NO_3)_4$, 8 M, HNO_3	18064.4	2.1	18069.1	1.84	2.46
Pu(IV), $(NO_3)_6^{2-}$, 13 M HNO_3	18063.8	1.5	18068.6	1.80	2.49
Pu(IV), $(NO_3)_6^{2-}$, CH_3CN	18063.9	1.6	18068.5	1.85	2.48
Pu(IV), $(NO_3)_6$ (xtal)	18063.8	1.5	18068.5	1.84	2.48
		Carbonato Complexes			
Pu(IV) $(CO_3)_5^{6-}$ (solution)	18063.2	0.9	18067.8	1.78	2.43
Pu(IV) $(CO_3)_5^{6-}$ (solid)	18063.6	1.3	18068.6	1.64	2.43
$Pu(V)O_2(CO_3)_3^{5-}$	18062.9	0.6	18067.2	1.46	1.84, 2.50
$Pu(VI)O_2(CO_3)_3^{4-}$ (solution)	18064.7	2.4	18069.4	1.46	1.75, 2.48
$Pu(VI)O_2(CO_3)_3^{4-}$ (solid)	18065.0	2.7	18069.8	1.40	1.77, 2.46
		Hydroxo Complexes			
(VI) 1 M $HClO_4$)	18064.9	2.6	18069.5	1.47	1.76, 2.41
$PuO_2(OH)_4^{2-}$, 2.2 M LiOH	18063.9	1.6	18069.3	1.44	1.81, 2.30
$Pu(VII)O_{2+x}(OH)_y$	18065.4	3.1	18071.5	1.42	1.78, 2.28
		Pu(IV+) Oxy-hydroxides			
PuO_2	18062.3 ± 0.3	reference	18068.6 ± 0.3	1.55	2.33
(IV), 1 M $HClO_4$	18063.2	0.9	18068.7	1.72	2.39
nitrate	18063.0	0.7	18068.7	1.70	1.83, 2.22, 2.38, 2.84, 3.05, 3.29
nitrate + NaCl	18063.1	0.8	18068.7	1.69	1.86, 2.21, 2.36, 2.84, 3.04, 3.28
nitrate + citrate	18063.5	1.2	18068.8	1.72	1.83, 2.23, 2.39, 2.82, 3.06, 3.31
aged	18063.4	1.1	18068.6	1.66	1.88, 2.19, 2.35, 2.77, 3.04, 3.31
aged hydrothermal	18062.8	0.5	18068.6	1.54	1.82, 2.19, 2.36, 2.78, 3.03, 3.32
reduced (VI): Fe	18063.4	1.1	18069.1	1.70	1.84, 2.25, 2.38, 2.80, 3.01, 3.33
reduced (VI): Fe + NaOCl	18063.3	1.0	18068.6	1.73	2.25, 2.37, 2.78, 3.04, 3.32
reduced (VI): Al	18063.6	1.3	18069.0	1.71	2.23, 2.38, 2.84, 3.02
reduced (VI): Al + NaOCl	18063.5	1.2	18068.7	1.71	2.16, 2.30, 2.44, 2.86, 3.06, 3.32
high fired (a)	18062.2	−0.1	18068.8	1.50	2.26, 2.36, 2.76, 2.98, 3.27
$x = 0.17$	18063.1	0.8	18069.8	1.45	1.91, 2.35, 2.71, 2.94, 3.31
$x = 0.21$	18062.4	0.1	18069.2	1.44	1.93, 2.21, 2.33, 2.74, 2.97, 3.30
$x = 0.26$	18061.6	−0.7	18068.6	1.43	1.84, 2.13, 2.28, 2.41, 2.73, 2.94
low fired	18062.2	−0.1	18068.9	1.45	2.27, 2.39, 2.68, 2.86, 3.07, 3.31
high fired (b)	18061.2	−1.1	18068.2	1.39	1.88, 2.28, 2.38, 2.78, 3.34
15% humidity	18062.0	−0.3	18068.6	1.46	1.85, 2.14, 2.32, 2.81, 3.34
37% humidity	18062.4	0.1	18068.6	1.53	1.89, 2.13, 2.26, 2.37, 2.72, 2.97
80% humidity	18062.2	−0.1	18068.7	1.47	1.88, 2.19, 2.33, 2.77, 3.33

Table 1. (Continued)

sample	edge energy	ΔeV PuO_2 edge	peak energy	normalized peak height	nearest neighbor Pu−X distances (Å)
Pu(IV+) Oxy-hydroxides Substitional Pu-Containing Oxides					
(III) 1 M $HClO_4$	18060.0	−2.3	18064.3	1.85	2.48
(IV) 1 M $HClO_4$	18063.2	0.9	18068.7	1.72	2.39
$Nd_{0.5}Pu(III)_{0.5}PO_4$	18059.1	−3.2	18064.3	1.64	2.46
$Ca_{0.8}Pu(III)_{0.2}HfTi_{1.8}Al_{0.2}O_7$	18059.0	−3.3	18064.7	1.62	2.38, 2.87
$Ca_{0.8}Pu(IV)_{0.2}HfTi_{1.8}Al_{0.2}O_7$	18062.7	0.4	18069.0	1.68	2.34, 2.85
$Ca_{0.9}Pu(III)_{0.1}Ti_{0.8}Al_{0.2}O_3$	18059.3	−3.0	18063.8	1.57	2.31
$Ca_{0.9}Pu(IV)_{0.1}Ti_{0.8}Al_{0.2}O_3$	18062.6	0.3	18068.2	1.54	2.25, 2.85
Pu(IV) in borosilicate glass	18063.2	0.9	18069.4	1.66	2.23

[a] Edge inflection point (edge energy) of ordered PuO_2 = 18062.3 eV based on first inflection point of Zr metal = 17999.35 was used as the reference for comparison with the energies of other compounds.

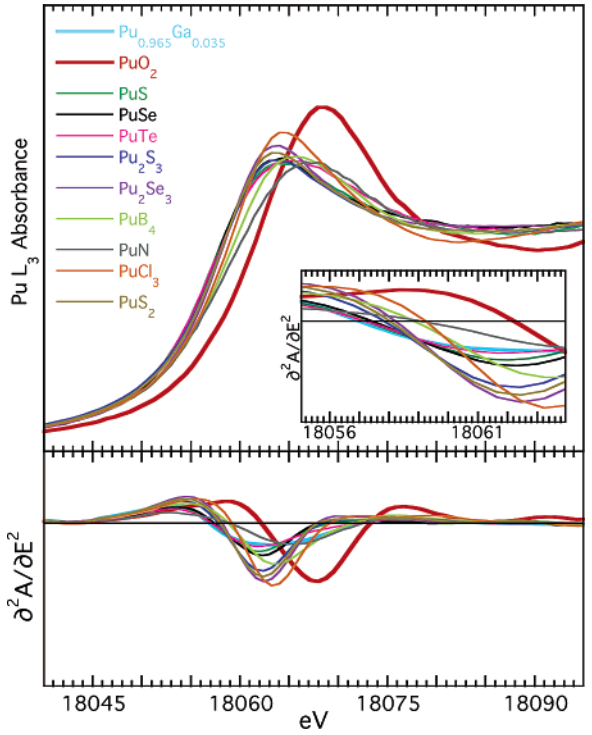

Figure 2. XANES (normalized absorbance, top; second derivative, bottom; expanded zeros of second derivative, inset) of Pu(III,IV) chalcogenides, boride, chlorides, and nitride. The spectra of δ PuGa and PuO_2 are included for comparison. The vertical scales of the absorbance and second derivative are identical to those in Figure 1.

part of the coherent structure. The most notable characteristic is the very low energies of the edges of all of the valences, which approach that of the metal, and the peaks, which are well below that of the metal (Figure 2). The edges of the sulfides are all 2−3 eV below that of the Pu(III) aquo complex and within 0.2−1.0 eV of the metal. Despite the edges of all three sulfide compounds being within 0.8 eV of each other, the energies of the Pu(II, III, and IV) do follow the expected order, as do the Pu(II) and (III) selenide and Pu(II) and (IV) telluride, demonstrating the high accuracy possible in the measurement. The energy of the Pu(IV) sulfide edge is only marginally higher than that for (III) sulfide, and both it and the edge of the Pu(IV) telluride are below that of the (III). Along with the Pu(II) compounds, the energies thus fall as sulfide < telluride < selenide, although the differences are at the limits of the experimental precision. The amount of electron transfer from the divalent higher chalcogenides must be quite significant, contributing to the semiconducting or partially metallic character of these compounds. The peak amplitudes (and that of the boride) are also low, which may be an effect of the backscattering amplitude function that extends to higher energy than for the lower *Z* elements. In contrast, the spectra of the chloride complexes are more normal, with a higher, narrower peak. The −0.8 eV difference between the edge energies of the Pu(III) chloride and (III) aquo is now smaller than the −1.8 eV shift between the corresponding Pu(IV) complexes, and the 2.2 eV difference between the Pu(III) and (IV) chloride compounds approaches the 3.2 eV difference between the edge energies found for the Pu(III) and (IV) aquo ions. The different Pu−O and Pu−Cl distances and EXAFS frequencies may contribute to these differences between the aquo and their corresponding chloride spectra. The peak amplitude in the sulfide, selenide, and boride spectra is modest compared with those of PuO_2 and the Pu(IV) chloride as well as being lower than that of the (III) chloride. The low energy, narrow, asymmetrically fast rising peaks appear to be characteristic of most Pu(III) spectra, with some exceptions such as the boride. This may reflect the inhomogeneity of the boride sample.

Aquo-Chloride Complexes in Acidic Media. This series of (IV) and (VI) chloride complexes shows the effects of continuously replacing oxygen atoms from aquo ligands with Pu−O distances of 2.39 Å with larger, higher *Z* chloride (Pu−Cl = 2.62 Å) by increasing the chloride concentration in the solution. This is shown in **C** for the trans dioxo Pu(VI) species, except that full substitution of the equatorial ligands is difficult to attain in solution. The Pu(IV) behavior is

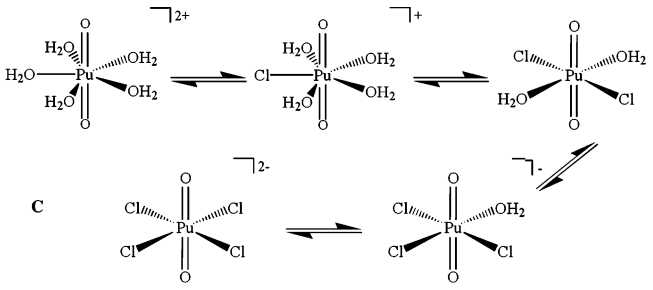

completely analogous, except that higher Cl/O ratios are attained in solution and since there are no equivalents to the oxo groups all of the ligands are exchangeable. The Pu−O and Pu−Cl distances are very similar in both valences and across the entire range of Cl/O ratios. These substitutions

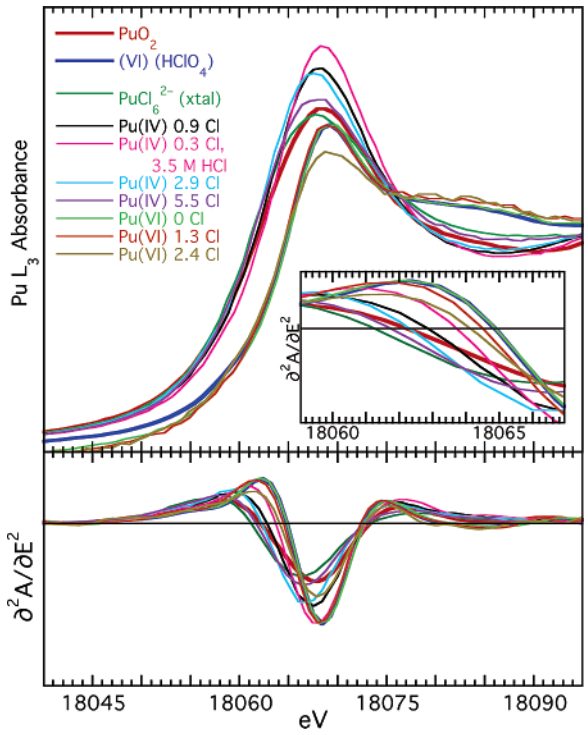

Figure 3. XANES (normalized absorbance, top; second derivative, bottom; expanded zeros of second derivative, inset) of Pu(IV,VI) chloride complexes. The legend lists the number of coordinated Cl^-; the remaining ligands are H_2O. The spectra of PuO_2 and $PuO_2^{2-}(H_2O)_4$ are included for comparison. The vertical scales of the absorbance and second derivative are identical to those in Figure 1.

do not significantly alter the normal characteristics of the (IV) and (VI) spectra. What both valences do display is a decrease in peak height and edge energy with increasing numbers of chloride ligands. In addition, the height of the shoulder in the (VI) spectra is somewhat higher for the chloride complexes (Figure 3). The peak widths for the species with Cl/O ratios close to one may be somewhat broader than those with more homogeneous neighbors, which would be expected for an EXAFS wave. A notable effect for Pu(IV) is that, although in 3.5 M HCl with added $NaClO_4$ only a trace or negligible amount of chloride is coordinated to the Pu, there is nevertheless a slight (0.5 eV) increase in the edge (but not peak) energy and peak amplitude relative to the Pu(IV) aquo ion in 1.0 M $HClO_4$ and no decrease in peak height consistent with peak broadening. This implies that the medium, specifically, changes in ionic strength and H^+ activity, can modify the XANES of compounds with identical coordination environments by amounts comparable to chemically significant changes in speciation. The spectra of the Pu(IV) aquo complex in 1 M $HClO_4$ and 1 M $HClO_4$/1 M NaCl are also identical. This indicates that any differences in speciation (specifically, the numbers of chlorides) are below the EXAFS detection limit. The edge shifts with increasing numbers of chloride ions are small individually, but monotonic and large and approximately even over the total substitution range. For Pu(IV), the edge energy decreases by −1.8−2.3 eV upon replacing six O atoms with six Cl^-, depending on the selection of the starting complex. For Pu(VI), the edge decreases by 0.8 eV going from zero to 2.4 equatorial chloride ligands. Ignoring the possibility of medium effects, the shift of −0.3 eV/chloride is similar for both Pu(IV) and (VI). The propensity of the chloride anion to reduce both the edge energy and peak amplitude in these spectra is therefore unambiguous.

Pu(IV) Nitrato Complexes. The Pu(IV) state will coordinate with up to five or six nitrate ions in concentrated nitric acid (**D**), giving it a total coordination number of 10−12, larger than with monodentate ligands. It is currently thought

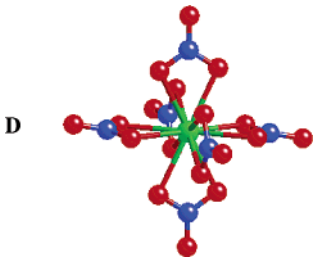

that although the hexanitratro complex is produced by crystallization from high concentrations of nitric acid, the solutions contain a mixture of penta- and hexa-nitrato species at the maximum acid concentration.[60] Pu(V) and (VI) oxo complexes and Pu(IV) also have a strong affinity for carbonate over a range of less extreme conditions, with the difference that the carbonato ligand is doubly instead of singly charged. The Pu−O(nonoxo) distances in all of these complexes fall in a relatively narrow range, 2.42−2.50 Å, with the longer distances occurring with higher coordination numbers as steric constraints force an expansion of the coordination shell. Curiously, the Pu−N and Pu−distal O distances of the (IV) nitrato complexes do not change in parallel, nor is there any sign of increased disorder in the nearest neighbor O distribution.[30] The peak heights of the Pu(IV) nitrato XANES spectra are significantly larger than that of the pure aquo complex, with the maximum found for the bis-nitrato complex (Figure 4). The most remarkable effect, however, is the shift to higher energy. The edge (and peak) energy for the bis-nitrato complex is actually 0.5 eV higher than that of the Pu(VI) aquo species and the hexa-nitrato spectrum 0.6 eV above that of the (IV) aquo. The maximum shift of the edge energy relative to the aquo species is therefore 2.2 eV and largest expansion of the Pu−O distance 0.10 Å, with the most extreme energy shift belonging to the bis-nitrato and not the hexa-nitrato species, which does however exhibit the largest change in distance. This is not easy to understand, since if it were only dependent on the charge then the aquo complex with no coordinated anions would have the highest instead of the lowest energy. It may therefore be a combination of the formal charge and some effect of the medium. The magnitude of the pure charge effect on the bis-, tetra-, and hexa-nitrato complexes, −0.4 eV/nitrate, is comparable to that of chloride. As was observed for the aquo complex in HCl and higher ionic strength, this

(60) Keogh, D. W.; Tait, C. D.; Clark, D. L.; Gordon, P. L.; Hawkins, H. T.; Palmer, P. D.; Scott, B. L.; Veirs, D. K. Selective crystallization and characterization of the technologically important $\{Pu(NO_3)_6\}^{2-}$ species. *Abstracts of Papers of the American Chemical Society*, National Meeting of the American Chemical Society, Chicago, IL, 2001; American Chemical Society: Washington, DC, 2001.

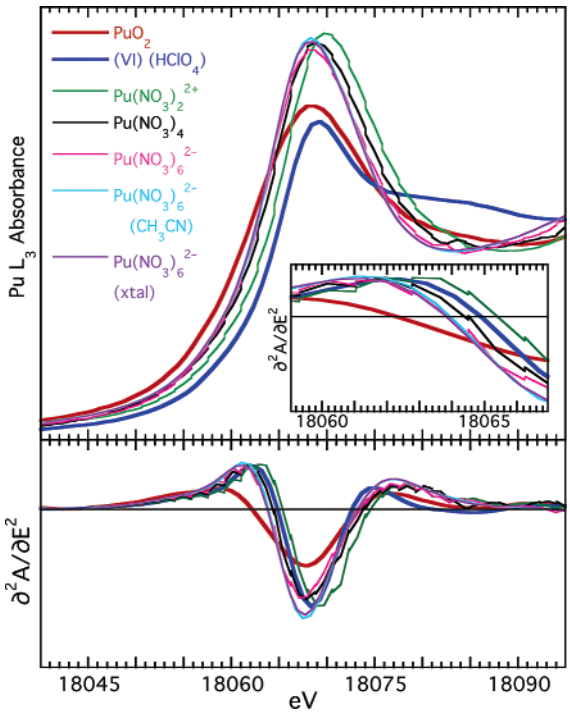

Figure 4. XANES (normalized absorbance, top; second derivative, bottom; expanded zeros of second derivative, inset) of Pu(IV) nitrato complexes. The jagged points are where, with an older data acquisition program and monochromator, duplicate points were collected because the requested interval was less than one motor step. The spectrum labeled "$Pu(NO_3)_6^{2-}$" is now believed to be most like a mixture of the penta- and hexanitrato complexes, with the former predominating.

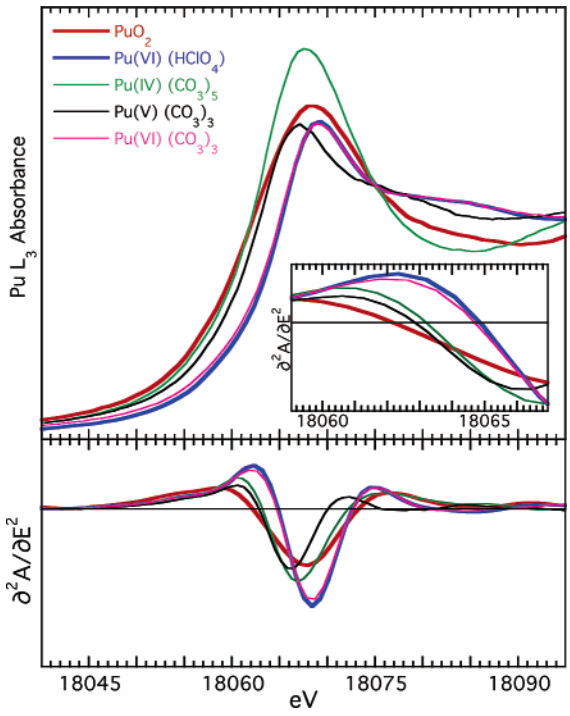

Figure 5. XANES (normalized absorbance, top; second derivative, bottom; expanded zeros of second derivative, inset) of Pu(IV,VI) carbonato complexes. The second derivative zeros correspond to the inflection points of the absorption edge and are used as the edge energy. The spectra of PuO_2 and $PuO_2^{2-}(H_2O)_4$ are included for comparison. The vertical scales of the absorbance and second derivative are identical to those in Figure 1.

medium effect appears to be larger for the ions coordinated only with neutral aquo ligands that result in the maximum positive charge for the complex. The edge and peak energies of the hexa-nitrato spectra are identical in 13 M HNO_3, acetonitrile, and in crystalline form, although the peak amplitude may be somewhat suppressed in aqueous solution. The rapid rise of the edge decreases the separation between the edge and peak energies relative to the aquo and chloro spectra.

Carbonato Complexes. The Pu(V) and (VI) (**F**) carbonate species exhibit behavior analogous to the Pu(IV) with the same ligand (**E**), coordinating up to three carbonates in the equatorial plane to form complexes with a two oxo + six equatorial configuration for a total coordination number larger than that for monodentate ligands. In addition to the stronger binding of the divalent carbonate ligand relative to the nitrate, the Pu(IV) complex saturates at five carbonates compared to six nitrates. In contrast to the nitrates, the spectra of the more anionic Pu(IV) and (VI) carbonato complexes in their near neutral solutions both show a small, −0.4 eV decrease in energy and higher peak amplitudes relative to their solids (Figure 5). Despite its 0.05 Å shorter Pu−O distance and greater negative charge, the Pu(IV) carbonate solid edge and peak energies are within 0−0.2 eV of those of the hexanitrato species (these values are reduced in solution), as are the energies of the Pu(VI) complex despite its larger coordination number and change in charge from 2+ to 4−. The 1.4−1.5 eV differences in the edge and peak energies between the Pu(IV) and (VI) solution and solid carbonato complexes are comparable to the 1.7 eV difference for the edge energy of their aquo counterparts. Since the Pu(V) carbonate edge energy is shifted to higher energy by 0.6 eV relative to its corresponding aquo species, the Pu(IV)−(V) and (V)−(VI) changes are smaller. The general for lower edge energies for Pu(V) compared to (IV) is retained. Overall, the valence dependent energy shifts in the edge are similar to those for the other types of complexes, and similar to the nitrates, the peak energies may be marginally closer to the edges than for the aquo and chloro species. The shapes of the Pu(V) and (VI) spectra are essentially identical to those for the aquo species. The overall behavior is quite similar to the nitrates, with the greater negative charge of the carbonate ligand possibly effecting slightly lower energies for the Pu(IV) complexes.

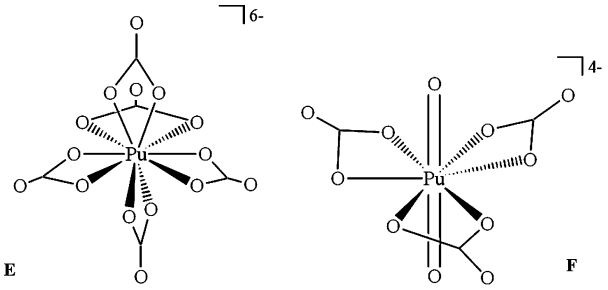

Hydroxo Complexes. Actinyl complexes in alkaline media (**G**, **H**) are characterized by expanded oxo bond lengths and contracted An−OH equatorial distances and a variable number of equatorial ligands.[61,62] Hydroxide ligation also helps stabilize higher valences. In the case of homogeneous ligation, Np(VII) occurs as the tetraoxo complex.[28]

Mixed hydoxo-carbonato Np(VII) compounds, however, display the standard dioxo configuration.[62] The competition between these two conformations and the sensitivity of structure and speciation to *Z* have left open the question of the structure of Pu(VII), which we have very recently found to be dioxo in the pure hydroxide compound at high base concentrations.[63] Consistent with the EXAFS interpretation of the edge, the distinctive high energy shoulder typical of oxo species is altered (Figure 6). The peak is somewhat lower and broader, and the shoulder is elevated so that the two features begin to merge and be less resolved. The other significant difference in the XANES is the decrease in the energy of the edge, by 1.0 eV for the Pu(VI) hydroxo complex in comparison with the corresponding aquo complex. This is similar to what has been observed in the spectra of neptunyl hydroxide complexes, and may signify additional electron donation from the hydroxide ligands at short distances.

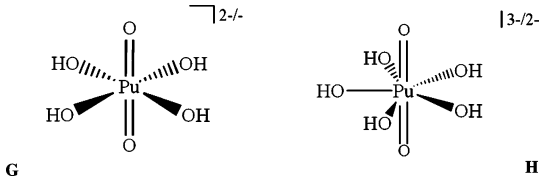

G H

Pu(IV,V) Oxy-hydroxide Compounds. $PuO_{2+x-y}(OH)_{2y}\cdot H_2O$ compounds are derivatives of PuO_2,[64] which has the cubic, fluorite-type structure (**I**). They are easily prepared, often in colloidal form, via precipitation of Pu from solution by neutralization/hydrolysis or by reduction of the more soluble higher valences. They can also be prepared by oxidation of PuO_2 with H_2O at elevated temperature. Their diffraction patterns are identical to that of PuO_2, except that they often give indications of disorder and a slight increase in the lattice parameter with increasing *x* has been observed.[65] Local structure measurements have found that the excess O atoms occur as oxo groups with rather long (1.83−1.91 Å) Pu−O distances and that the O sublattice displays a multisite distribution even in compounds with no excess O. The elongated Pu═O bonds in tandem with the (absence of) energy shifts of the XANES relative to the spectra of pure PuO_2 and in comparison with the spectra of certain Pu(V) and (VI) compounds indicate that the excess charge in materials with $x > 0$ is localized on $Pu(V)O_2^+$ moieties.[64,66] The retention of the (X-ray) diffraction pattern is accounted for by the observation that the Pu sublattice is conserved locally, albeit with evidence for Pu disorder around a single average site but with no sign of additional Pu locations in the lattice.[67] The O shell of PuO_2 (Pu−O = 2.33 Å) is broken up into a multisite distribution, with several distinct, separated subshells at specific distances that tend to be nearly the same in compounds prepared by both both high-temperature gas-phase reactions with solid PuO_2-type compounds and by hydrolytic or reductive precipitation from aqueous solution. In addition to the 2.33 Å Pu−O distance of PuO_2, there are shorter distances similar to those found for Pu−OH, implying protonation of some of the oxide anions and a subsequent shift in bonding (**J**). There are also a number of longer Pu−O distances extending out to 3.5 Å, so that the best description of the structure may be as a conglomeration of Pu(IV) (and PuO_2^+ when $x > 0$) oxy-hydroxide-aquo units oligomerized via various bridging moieties in which the Pu locations average to the same sublattice as in PuO_2 and the O atoms are locally ordered with discrete bond lengths for each species but show very poor long range order.

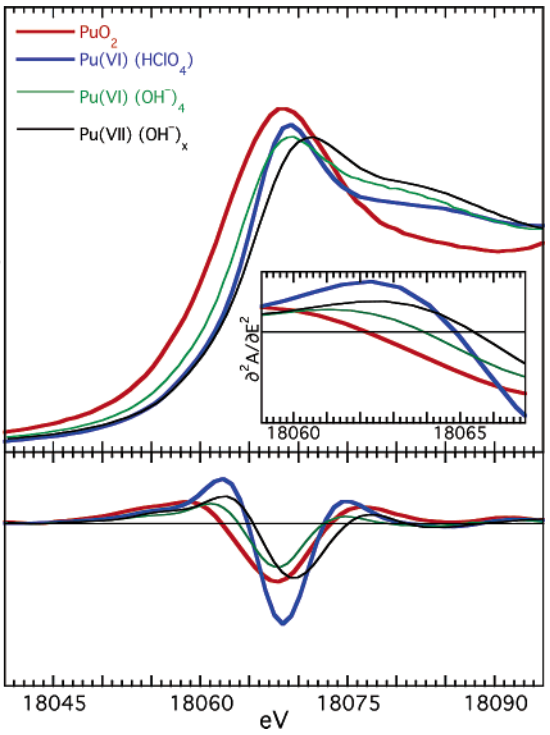

Figure 6. XANES (normalized absorbance, top; second derivative, bottom; expanded zeros of second derivative, inset) of Pu(VI,VII) hydroxide complexes. The spectra of PuO_2 and $PuO_2^{2-}(H_2O)_4$ are included for comparison. The vertical scales of the absorbance and second derivative are identical to those in Figure 1.

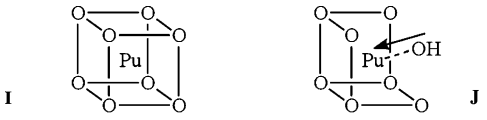

I J

The XANES from this $PuO_{2+x-y}(OH)_{2y}\cdot H_2O$ series serves as a demonstration and warning about how particular subtle and even unknown structural parameters can be the deter-

(61) Clark, D. L.; Conradson, S. D.; Donohoe, R. J.; Keogh, D. W.; Morris, D. E.; Palmer, P. D.; Rogers, R. D.; Tait, C. D. *Inorg. Chem.* **1999**, *38*, 1456.
(62) Clark, D. L.; Conradson, S. D.; Neu, M. P.; Palmer, P. D.; Runde, W. H.; Tait, C. D. *J. Am. Chem. Soc.* **1997**, *119*, 5259.
(63) Conradson, S. D.; Clark, D. L.; Gordon, P. L.; Keogh, D. W.; Tait, C. D. *J. Am. Chem. Soc.*, manuscript in preparation.
(64) Conradson, S. D.; Begg, B. D.; Clark, D. L.; Den Auwer, C.; Espinosa-Faller, F. J.; Gordon, P. L.; Hess, N. J.; Hess, R. F.; Keogh, D. W.; Morales, L. A.; Neu, M. P.; Runde, W. H.; Tait, C. D.; Veirs, D. K.; Villella, P. M. *Inorg. Chem.* **2003**, *42*, 3715.
(65) Haschke, J. M.; Allen, T. H.; Morales, L. A. *Science* **2000**, *287*, 285.
(66) Conradson, S. D.; Begg, B. D.; Clark, D. L.; den Auwer, C.; Ding, M.; Espinosa-Faller, F. J.; Gordon, P. L.; Haire, R. G.; Hess, N. J.; Hess, R. F.; Keogh, D. W.; Morales, L. A.; Neu, M. P.; Paviet-Hartmann, P.; Runde, W. H.; Tait, C. D.; Veirs, D. K.; Villella, P. M. *J. Am. Chem. Soc.*, submitted for publication.
(67) Conradson, S. D. *Appl. Spectrosc.* **1998**, *52*, A252.

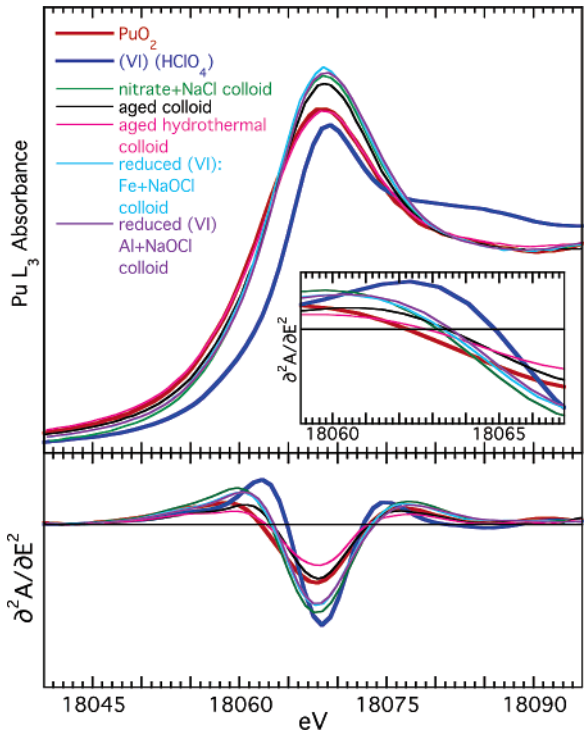

Figure 7. XANES (normalized absorbance, top; second derivative, bottom; expanded zeros of second derivative, inset) of indicated $PuO_{2(+x)}$ oxyhydroxide compounds prepared from aqueous solution. The vertical scales of the absorbance and second derivative are identical to those in Figure 1.

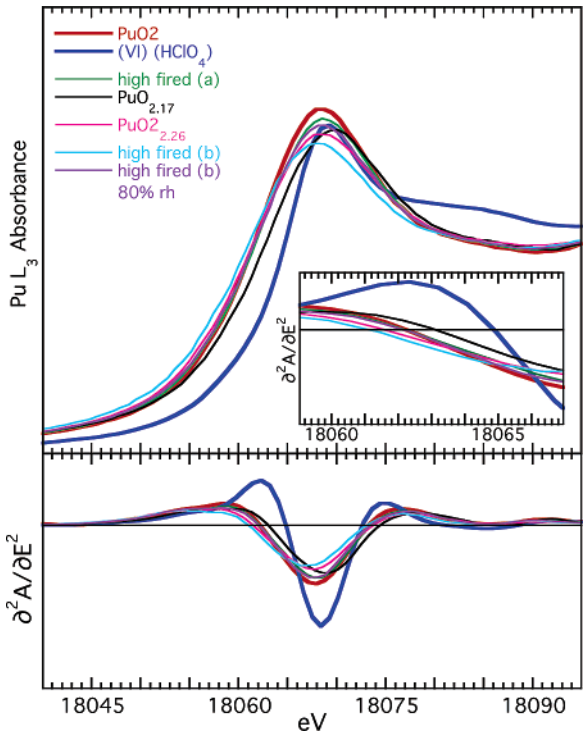

Figure 8. XANES (normalized absorbance, top; second derivative, bottom; expanded zeros of second derivative, inset) of $PuO_{2(+x)}$ oxyhydroxide compounds prepared by reaction at elevated temperature. The vertical scales of the absorbance and second derivative are identical to those in Figure 1.

minants of the spectrum, obviating the extraction of more obvious and useful correlations between, e.g., charge and peak amplitude. The spectra of samples precipitated from H_2O by both hydrolysis and reduction, with the exception of the hydrothermally treated one, have main peaks with 0.11−0.17 higher amplitudes, 0.7−1.3 eV higher edge energies, and peak energies as much as 0.5 eV higher than those of ordered PuO_2 (Figure 7). The spectra of samples prepared with treatments at elevated temperature, including hydrothermal, show main peaks that are lower by 0.01−0.16, edge energies shifted by −1.1−0.8 eV, and peak energies shifted by −0.4−1.2 eV (Figure 8). It might therefore be expected that these compounds display a trend in structure or charge such that ordered PuO_2 falls between the other two sets. This is however, not the case. The EXAFS of the heat treated materials do tend to show fewer O atoms with Pu−O > 2.5 Å and some tendency toward narrower distributions and larger Pu amplitudes.[64,66] Not only is there overlap of these structural characteristics between the two sets but also within each set there is no trend in the spectra associated with these characteristics. This is also the case for the average Pu charge determined by the numbers of excess O atoms with Pu−O < 1.9 Å.[64,66] There is, therefore, no correlation between the spectral features and these aspects of the Pu speciation, posing the question of what is the origin of this rigorous relationship between the XANES and the method of preparation.

Some spectral and speciation parameters can be described. Since the peak energies are relatively invariant, the inverse correlation between peak amplitude and edge energy could simply reflect a broadening of the peak. However, the trailing edges of the peaks are not correspondingly shifted, so if there is such a pattern then all of the change in shape occurs on the leading edge and the peaks are becoming less symmetric. A similar study of ThO_2 made from aqueous solution also found similar amplitude changes pointing to the main peak amplitude as a variable in the spectra of An(IV)O_2 compounds, although the broadening was ambiguous.[8] Two parameters originating in the mixed Pu valence that could be expected to contribute to the energies and peak amplitude are the following: Pu(V) spectra are shifted slightly to lower energy; and Pu-oxo complexes have lower peak amplitudes and are broader because of the interference in the EXAFS between the two waves from the two separate O shells, an effect that diminishes when the difference in the two Pu−O distances decreases. There are, however, no definite correlations between peak amplitude, edge energy, and the energy of the backside of the edge with the number of oxo groups. Ignoring the spectrum of ordered PuO_2, the structural features most closely associated with lower main peaks and edge energies are the amplitude of the Pu nearest neighbor contribution in the $\chi(R)$ spectrum and the width of the O shell centered at 2.33 Å in the radial distribution function. The annealing that occurs at the elevated reaction temperature tends to increase both the O and Pu ordering, and the spectra of these compounds have lower peaks with edges shifted to lower energy in their XANES. Interference between the Pu−Pu and Pu−O waves in the EXAFS that is maximally destructive at the peak would then explain this correlation and the difference between the aqueous and heat treated materials. The Pu−Pu wave is in fact out of phase with Pu−O at low k and descending at $k = 0$, but the Pu−Pu

amplitude is significantly lower than Pu−O below $k = 3$ Å^{-1} and it is not obvious why the Pu contribution to the EXAFS and its reducing effect on the XANES would increase faster than the O contribution and its enhancing one. What this association with order does not explain, though, is the variations within the sets or the placement of the ordered PuO_2 spectrum between these other types.

The absence of a clear pattern relating the structure to the XANES and the structural and chemical complexity of the $PuO_{2+x-y}(OH)_{2y}\cdot H_2O$ make it difficult to understand these effects, most likely because they compete with each other and tend to cancel each other out in the spectra. It is also difficult to identify samples that differ by only one structural parameter. The average nearest neighbor distance in the oxyhydroxides is close to that in PuO_2 and shorter than that in the aquo species, especially when weighted by $1/r^2$. As already described, the O^{2-} and OH^- groups are much more polarizable and effective at donating electrons to the Pu than are the H_2O ligands. It may be that, although they are better, the disorder results in fewer of them so that their total ability for neutralizing the charge on the Pu and lowering the edge energy is less, even while the inverse square weighting in the EXAFS increases the amplitude at low k for the atoms in the Pu coordination sphere before the Debye−Waller factor damps it at higher k. What is clear is that the sum effect of the extended disorder and change in valence can both effectively broaden and narrow the peak with small or negligible changes in the peak position but significant changes in its shape that modify the edge energies and peak amplitude. Another, somewhat speculative, possibility is stereochemistry. Shifting of spectral weight between the L_2 and L_3 edges has been described.[16] We have observed in Pt L_3 edges that the white line amplitude varies more between some cis- and trans-diammine complexes than it does between some Pt(II) and (IV) ones.[68] Treatment at elevated temperature could conceivably promote the transformation of these complexes with their complicated coordination environments into a more stable three-dimensional configuration even while the one-dimensional description from the EXAFS remains unchanged.

Substitutional (III)/(IV) Oxides. Pu can also form solid solutions in certain oxide minerals and borosilicate glass, with its site in the crystalline compounds determined by the overall stoichiometry. Once incorporated, its valence can be controlled by annealing at elevated temperature under reducing or oxidizing conditions, producing Pu(III) and (IV), respectively. Pu(III)−O nearest neighbor distances are around 0.05 Å longer than the Pu(IV)−O distances in the same compounds, compared with the 0.09 Å difference between the aquo species in $HClO_4$. These Pu−O distances are also often contracted by more than 0.1 Å compared with the aquo species, but the EXAFS measurements also show they are often split into a set of atoms at 2.25−2.35 Å and a smaller number of O atoms at 2.85−2.95 Å. The overall Pu−O distribution is therefore quite different from the multitude of shorter distances found in the oxyhydroxides. The Pu in

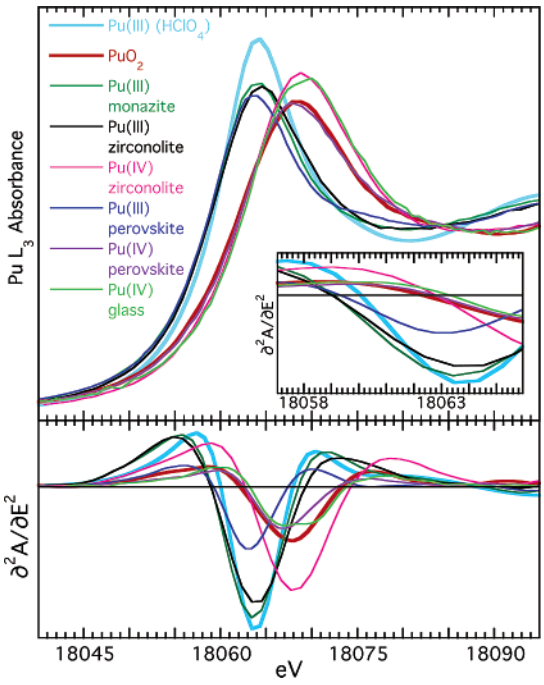

Figure 9. XANES (normalized absorbance, top; second derivative, bottom; expanded zeros of second derivative, inset) of Pu(III,IV) substituted into oxides and glass. The spectra of PuO_2 and Pu(III)(8−10)(H_2O) are included for comparison. The vertical scales of the absorbance and second derivative are identical to those in Figure 1.

the glass displays only a single, relatively short distance. Although not as homogeneously ordered as are most of the other compounds in this study, these materials are nevertheless useful for testing the effects of additional types of local environments. The edge energies of the Pu(III) samples are close to that of the (III) chloride and almost 1 eV below that of the aquo species, perhaps as a result of the contracted bond length (Figure 9). The peak energies, however, can be closer to that of the aquo, with a broader overall peak and shallower leading edge. The diminished peak heights may reflect the smaller number of O neighbors in the minerals. The peak heights from the Pu(IV) species, like those of the oxyhydroxides, are usually higher than that from PuO_2, although not as dramatically as for the nitrato complexes with their very large number of coordinated O atoms. In contrast to these other species, however, the shift in the edge relative to PuO_2 is lower, only around 0.5 eV, although they are similar in showing the same peak energy. Overall, there is no distinct correlation between lower energy and Pu−O distance in this set of compounds. One possible explanation is that the details of the bonding modes, involving, e.g., OH^- or OR^- bound to one or two Pu sites vs an O^{2-} placed symmetrically between four Pu ions, are comparably important to the bond length effects. The types and numbers of extended neighbor atoms involved may also play a role. The effectiveness of bonded OH^- in reducing the Pu charge may be different than that of −O−Si−O−, and the Ca, Hf, Ti, and Al cations are likely to display different affinities for the charge on the O atoms than the Pu. The somewhat different energy trends displayed by these compounds therefore continue to point to the significance of all aspects of the local environment in determining the particulars of

(68) Conradson, S. D. Unpublished results.

the XANES, while simultaneously corroborating that the more general attributes of the spectrum are largely invariant.

Discussion

This extended set of spectra confirms the utility of XANES for determining Pu (and therefore other actinides) valence and certain additional aspects of the speciation but also emphasizes the continued necessity of obtaining spectra of appropriate standard compounds. As described in the Introduction, the valence of an actinide is strongly coupled to its charge and coordination geometry and thus also correlated with the energies of the absorption edge and peak and to the shape of the spectrum across the edge. However, we have also now identified deviations from and modifications to this simple dependence of the XANES on the valence and local environment that could affect these types of interpretations. Thus, it is necessary to select appropriate standards to account for higher order effects. One relevant finding is that spectra of similar shapes obtained from samples with ostensibly similar local environments can exhibit sensitivity to their extended environments by displaying substantial energy shifts (Figure 10). These shifts are apparently larger for the inflection point than peak position, so that in the future it may be useful to prefer to use the peak to assign valence and the inflection point as a marker for secondary speciation differences. These shifts can be so large that spectra of essentially identical shape exhibit a range of energies greater than the variations among valences. There are examples of this resulting from both the characteristics of the medium in which the complex resides and other effects. The effect of ligand substitution can be equivocal; certain types of substitutions have minimal or negligible effects on the shape. These differences among spectra pose questions about the influence on the XANES of factors in addition to the valence and coordination environment, some of them unexpected. Since the shapes tend to agree at least qualitatively with calculations and be consistent with their assignment to low *k* EXAFS and associated unbound transitions, the outstanding issue to be addressed is therefore the energy shifts.

Comparison with XPS. Similar patterns in the observed trends, e.g., valence and ligand effects, found in other types of photoemission experiments would provide at least qualitative corroboration for some of the specific results from these XAFS. The anomalously small energy interval between (0) and (III) relative to the higher valences has been observed in XPS.[69,70] The 4f $^{7}/_{2}$ binding energy for Ga-stabilized δ Pu alloy occurs at 422.2 eV. The binding energies for Pu(II) O(C), Pu_2(III) O_3, Pu(IV) O_2, and Pu(IV) F_4 are, respectively, 1.4, 2.2, 4.3, and 7.3 eV higher than the metal. These are comparable with the Pu L_3 XANES results reported here of a 2.2−3.0 eV (0)−(III) increase for $PuCl_3$ and Pu(III) aquo relative to the metal, 5.3 eV for (0)−Pu(IV)O_2, and 3.1 eV for the largest difference between Pu(IV)O_2 and another Pu(IV) species. (It would obviously be of interest to have the XANES of PuF_4.) Cox and Farr[69] concluded that the

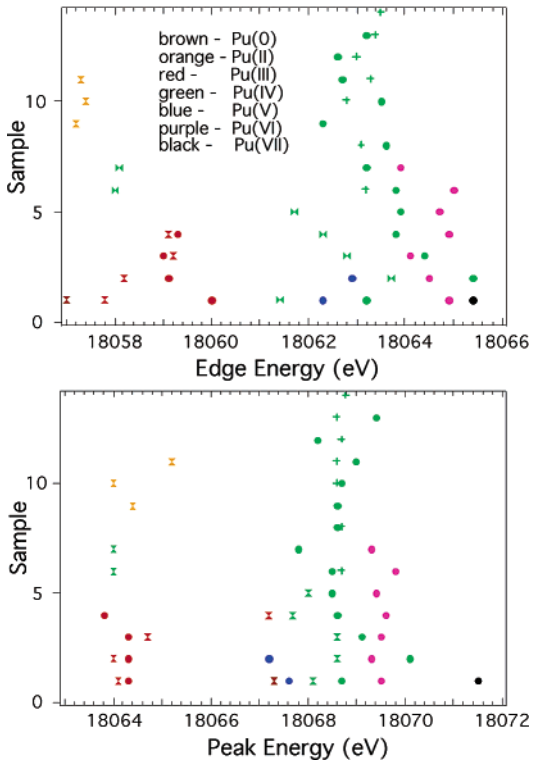

Figure 10. Histogram of occurrence vs inflection point (top) and peak (bottom) energies. Valence is indicated by color. Circles are compounds with only O in the first shell except that "+" indicates oxy-hydroxides (colloids); hourglasses are compounds with other atoms including mixed O−Cl coordination.

electron binding energies of actinides are most heavily influenced by primarily the 5f occupation from the initial valence plus the amount of charge transfer from the ligands (actual charge on An ion), and secondarily by the 5f-core level Coulombic interaction and final state screening energies. The second of these factors is only important in comparing results across the actinide row; the geometry of the f orbitals and extent of core penetration should be identical for all Pu compounds. Furthermore, when the relative energies of excitations probing initial states of different levels vary, it was stated that this is likely to originate in the last of these factors, e.g., the presence of the extra 6d electron and the amount of 5f screening in XAFS vs photoemission. Thus, differences in the core-hole screening mechanisms for metals and insulators would certainly provide one explanation for the much smaller energy shift per e^- between (0) and (III) relative to the shifts among the higher valence compounds. Screening effects will, however, be much smaller across sets of insulating compounds then between metallic phases and other compounds, so that the largest core-hole screening effect will be between metallic and insulating states. It is possible, however, that screening could be modified by metallic or semiconducting behavior in low or mixed valence materials, which was observed.

Semiconducting and Metallic Compounds. In the chalcogenides and halides, the valency might appear easy to assign on the basis of the formal Ch^{2-} and X^-, but this is not always the case. $PuCl_3$ is almost certainly close to trivalent, consistent with an edge energy 0.8 eV lower than

(69) Cox, L. E.; Farr, J. D. *Phys. Rev.* **1989**, *B39*, 11142.
(70) Farr, J. D.; Haschke, J. *Inorg. Chem.* **1981**, *20*, 1945.

that of the (III) aquo complex. We find PuB_4 and PuN close to this, and in the case of PuN this is expected. More difficult to assign are the compounds PuS, PuSe, PuTe, and (to a lesser extent) the sesqui-compounds Pu_2S_3 and Pu_2Se_3, the edge energies of which all converge on that of the metal. The understanding of the monochalcogenides is particularly controversial, with a number of competing theories for their behavior being promoted.[45,71] On balance, however, properties such as those derived from the photemission[43] and even bulk measurements[45] are indeed close to that of the metal. In this sense the edge energy confirms the general trends deduced from other measurements.

Edge energies below 18059−60 eV thus belong to condensed materials with delocalized charge where significant screening compresses the energies into a very narrow range that does not fall below the 18057 eV lower bound defined by the metallic state. Above this, the energies of the higher valence, insulating compounds display a much greater range because the localized charges are not as effective in shielding the core. Slight variations in the ability to promote metallic or semiconducting character might explain why the energies of the sulfides are lower than those of the selenides and tellurides even when their valence is higher, breaking the expected correlation between binding energies and ligand electronegativity that was reported for XPS and a more limited set of actinide compounds including pnictides.[4] Within these two regions of the edge energy/valence curve, electron donation from the ligands to the metal ion thus remains as the principal mechanism for modifying the binding energies. Ligand electronegativity/polarizibility has been used to explain the significantly higher XPS energy of PuF_4 relative to PuO_2.[69]

Ligand Polarizibility. This effect of ligand electronegativity or polarizibility on the energies is very much in evidence in these spectra. The special properties of the very short Pu−oxo bond account for the observation that the XANES of Pu(V) compounds are consistently lower than those of (IV). In addition, the substitution of chloride for aquo ligands lowers the energies of the XANES of both Pu(IV) and (VI) complexes monotonically and by similar amounts. These experiments also reveal some additional trends. The decrease in energies found for hydroxide complexes is consistent with a correlation between bond length and charge transfer to the Pu, although in this case it must be assumed that the expansion of the two Pu−oxo bonds has less effect than the contraction of the four or five equatorial Pu−hydroxo bonds. The coupling mechanism between the shift in energy and distance will certainly differ for the two types of bonds. In this regard it is also of interest to note that the Np(VI)−(VII) energy shift is around 1.1 eV (comparable to that for the same pair with Pu) and that this is the same for both the Np(VII) bis- and tetraoxo species that show the same edge energies despite their radically different geometries and bonding modes.[63] It is also evident that, for similar kinds of ligands at different distances, the one at the shorter distance is associated with lower XANES energies. However, since the moiety and bonding mode/length are correlated, it is only rarely possible to even qualitatively separate these two coupled effects. It is even possible to suggest a spectroscopic series for ability to lower the edge energy that is largely intuitively obvious: actinyl oxo > S^{2-}, Te^{2-} > Se^{2-} > B^{3-} > Cl^- > O^{2-} > OH^- > OSiO > CO_3^{2-} > NO_3^- > H_2O.

Effects of Local Disorder. After this, however, explaining the remaining patterns or trends displayed by these data becomes more complicated. Two effects can be identified, disorder and the medium. The XANES energies for Pu(III) substituting in oxides are significantly lower than for the aquo species. This is true even when the Pu−O distances are comparable to those in the aquo complex, so that this probably simply recapitulates the spectroscopic series with O^{2-} being more polarizable and a better electron donor than H_2O even at the same distance. The XANES energies, however, remain the same even in compounds where the Pu−O^{2-} distances are much shorter. In these cases, however, the local environments are disordered so that the Pu coordination sphere contains O atoms at very long as well as short distances.

This ambiguity pertains to Pu(IV) as well, and probably the underlying mechanisms. Nevertheless, the effects of disorder on the XANES of $PuO_{2+x-y}(OH)_{2y}\cdot H_2O$ are substantial. Oddly, considering how identical the behavior of all of the actinide XANES tends to be across the entire row, the enhanced amplitude of the main peak in the spectra relative to the parent PuO_2 of the more disordered compounds precipitated from aqueous solution exhibit the opposite trend to the ThO_2 system.[8] Since disorder for Pu can also diminish the amplitude, it is possible that this reflects identical spectroscopic but different chemical behavior.

One approach to the XANES from disordered environments could be that the contributions of the individual nearest neighbor atoms are additive. This is consistent with the other trends, such as chloride substitution. However, for a given number of nearest neighbors, the bond expansion undergone by some of them in order to allow others to come nearer to the central cation lowers the amount of charge transferred more than the amount gained by those whose proximity is enhanced. The cumulative effect of disorder, especially in a fixed volume, is therefore to increase the charge on the central atom and the energies of the XANES. Although the amounts are lower than the uncertainties for a single spectrum, the peak energies of all of the compounds actually are shifted up by an average of around 0.2 eV relative to that of ordered PuO_2. It is probably also important to consider that the disorder is associated with changes in speciation that may render the ligands less polarizable, e.g., protonation of O^{2-} to OH^-. Combined molecular dynamics−XANES calculations have demonstrated the importance of the details of the neighbor distributions on XANES, although with greater effects on spectral shape then energy.[72] These, however, included only thermal and not static contributions.

(71) Oppeneer, P. M.; Kraft, T.; Brooks, M. S. S. *Phys. Rev.* **2000**, *B61*, 12825.

(72) Merkling, P. J.; Munoz-Paez, A.; Pappalardo, R. R.; Marcos, E. S. *Phys. Rev.* **2001**, *B64*, 92201.

Another important characteristic of XANES exemplified by the Pu(IV) oxyhydroxides is the potential decoupling of the peak and edge energy shifts that can occur when the line shape is altered by chemical effects. This is consistent with a structural basis for the XANES where because the ionization energy is near the absorption onset the spectral features are determined by EXAFS and multiple scattering contributions and the main peak is not the transition to the 6d final state. It also shows, though, how sensitive this summation process can be since nuances in the local order can apparently affect not just the amount but also the direction that the peak amplitude changes. Finally, the possibility of the influence of three-dimensional ordering may also need be considered in the interpretation of the XANES.

Medium Effects. The other unexplained observation is that, apparently, the medium itself can have effects on the XANES energies that can be greater than valence. For those species where measurements have been performed on both solutions and solids, the energies and peak heights differ more often then they match. The surprising result, however, is the sensitivity of the energies to the composition of the solution for the nitrato and chloro complexes, even when other parameters such as bond lengths are unaffected. These energy shifts can be significantly larger than even those resulting from changes in valence. Higher acidities can produce much higher energies, with the possibility of some contribution from ionic strength as well. This effect is larger when the number of coordinated H_2O molecules is high, and in fact, anionic ligands, even ones that are low in the spectroscopic series, appear to shield the Pu from these medium effects. Saturating the Pu(IV) complex with nitrates in solution decreases the spectral energies by up to 1.6 eV relative to the bis-nitrato compound, to equal those of the hexa-nitrato complex in the solid and CH_3CN solution, even as the nitric acid concentration rises from 3 to 13 M. This effect is not easily understood. If higher acidities resulted in Pu coordinating with H_3O^+ instead of H_2O then some increase in bond length would be expected, but none is observed.

Concluding Remarks

In summary, these spectra corroborate the utility of XANES as a source of information on chemical speciation but do point to the necessity of being attentive to the use of the most appropriate standards. They also have described some new challenges for theorists in this area.

Acknowledgment. This work was supported by DOE NNSA/DP and OBES Division of Chemical Sciences under Contract W-7405 and (at Colorado State) DE-FG03-97ER14797. All experimental measurements were performed at the Stanford Synchrotron Radiation Laboratory, a national user facility operated by Stanford University on behalf of the U.S. Department of Energy, Office of Basic Energy Sciences. Health Physics support at SSRL was provided by the Los Alamos National Laboratory section of the Seaborg Institute for Transactinium Studies.

IC0346477